

Microscopic theory of scattering in imperfect strained antimonide-based heterostructures

M. J. Shaw

Department of Physics, The University of Newcastle upon Tyne, Newcastle upon Tyne, United Kingdom

(Received 6 October 1999)

A microscopic theory to provide quantitative predictions of scattering cross sections and carrier lifetimes in imperfect strained layer superlattices is developed. Strain-dependent empirical pseudopotentials are formulated to obtain the electronic wave functions with the results of scattering theory employed to extract the dynamical information. The theory is applied to a number of imperfect $\text{Ga}_x\text{In}_{1-x}\text{Sb}/\text{InAs}$ superlattices, containing isovalent substitutional anion defects, both isolated and in interface islands. Key factors governing the lifetime are identified, including defect atom type, location and lattice relaxation, and the detailed size and shape of the interface islands. Multiple scattering processes are shown to become significant for larger interface islands. Typical elastic scattering lifetimes for isolated antimony defects of $1.6 \mu\text{s}$ are predicted, dropping to 0.4 ns for islands containing approximately 50 defect ions.

I. INTRODUCTION

Over the past decade, enormous effort has been expended in the development of antimonide-based heterostructures consisting of layers containing GaSb, AlSb, and InSb, together with the lattice-compatible InAs. The motivation for this effort is the potential for applications in high-performance integrated optoelectronic devices operating in the infrared region of the spectrum,¹⁻¹⁸ and ultrahigh speed electronics.¹⁹⁻²¹ However, in spite of this effort these materials have failed to reach levels of performance sufficient to dislodge existing, though far from ideal, technologies. One of the principal reasons preventing the widespread application of the antimonide heterostructures is the lack of understanding of the fundamental physical processes restricting the carrier lifetimes.

Recently, advances in microscopy have provided a clear picture of the quality of structures and interfaces that can be achieved.²¹⁻²³ There is at present, however, no theoretical link between the microscopic disorder and interface distortion observed and the lifetimes in the device structures. A clear understanding of the role of imperfections of the lattice on a microscopic level in degrading the dynamic characteristics of devices is essential if the performance of antimonide heterostructures is to be improved. Recent studies using *ab initio* pseudopotential calculations have demonstrated that the microscopic properties of the interfaces are critical in determining the behavior of defects in these materials.²⁴ A theoretical model is required in which a microscopic description of defects and heterointerfaces is related to the essential dynamical properties which determine device performance.

Although there are a number of well-established methods for the description of the stationary-states in idealized antimonide heterostructures (e.g., $\mathbf{k}\cdot\mathbf{p}$, *ab initio* pseudopotential etc.), there is, to the author's knowledge, no existing scheme that lends itself to the description of *dynamical* properties of such structures in the presence of disorder on the microscopic level. This paper first develops an implementation of the empirical pseudopotential method applicable to strained superlattices (such as the antimonide-based structures), and then describes an approach whereby the results of scattering

theory are used to extract dynamical information from the stationary states of imperfect superlattices. The empirical pseudopotential provides a model that retains a microscopic atomistic description of the system, but that is sufficiently efficient to allow the perturbed states of the imperfect superlattice to be readily obtained by diagonalization. It is the ability to obtain the perturbed stationary states, which is exploited in the extraction of the dynamic properties such as scattering cross section and lifetime. The advantages of the empirical pseudopotential method over the commonly used $\mathbf{k}\cdot\mathbf{p}$ approach are detailed in a comparison of the two methods by Wang *et al.*²⁵

The theoretical scheme developed is applied to a typical antimonide heterostructure, a $\text{Ga}_{0.75}\text{In}_{0.25}\text{Sb}/\text{InAs}$ superlattice, originally proposed as an infrared detector. A range of imperfect structures is studied incorporating isovalent substitutional anion defects, known to be common in these structures,²³ and the dependence of scattering upon the microscopic details of the imperfections are analyzed. The results provide an essential first step towards an understanding of the role these defects play in limiting device performance, and ultimately towards an answer to the technologically important question of how the lifetimes in these structures may be improved.

II. EMPIRICAL PSEUDOPOTENTIAL CALCULATIONS OF STRAINED SUPERLATTICES

Before one can begin to consider the case of imperfect superlattices, it is first necessary to develop a reliable model to describe the idealized system. The basic requirements of this model are that it is at the same time atomistic in nature, as it is ultimately to be used to examine disorder/imperfections on a microscopic scale, and yet sufficiently simple to enable its practical application to systems with unit cells containing a very large number of atoms. The empirical pseudopotential method (EPM), in which a pseudopotential is obtained by fitting to empirical data for the bulk constituents (e.g., energy gaps, effective masses) is well established in the study of semiconductor superlattices over many years,^{26,27} and satisfies these basic demands. However, the

EPM was originally developed for application to lattice matched systems such as GaAs-Al_xGa_{1-x}As, and in its standard form is not applicable to strained superlattices such as the antimonides at the focus of this work. An EPM is formulated below in which strain-dependent empirical pseudopotentials are introduced allowing the extension of the EPM to a wide range of structures including the Ga_xIn_{1-x}Sb-InAs superlattices of particular interest.

In the first instance, for clarity, the strain-dependent EPM will be derived in the absence of spin-orbit coupling. The inclusion of spin to this method may then be achieved in the same manner as for the conventional EPM approach in the literature. The Hamiltonian of the system is written,

$$H = -\frac{\hbar^2}{2m}\nabla^2 + V_p(\mathbf{r}), \quad (1)$$

where the empirical pseudopotential $V_p(\mathbf{r})$ is assumed to be a local pseudopotential, dependent only upon \mathbf{r} . Defining a unit cell corresponding to reciprocal lattice vectors \mathbf{G} , the pseudopotential may be written in reciprocal space form,

$$V_p(\mathbf{r}) = \sum_{\mathbf{G}} \sum_i S_i(\mathbf{G}) V_i(\mathbf{G}) e^{i\mathbf{G}\cdot\mathbf{r}}. \quad (2)$$

Here, the structure factors $S_i(\mathbf{G})$ for each atomic species i contains the atomic positions,

$$S_i(\mathbf{G}) = \frac{1}{N_i} \sum_j e^{-i\mathbf{G}\cdot\mathbf{R}_j^i}, \quad (3)$$

and \mathbf{R}_j^i is the position of the j th atom of species i , and N_i is the number of atoms of species i . The terms $V_i(\mathbf{G})$ are the Fourier components of the atomic pseudopotentials, the form factors,

$$V_i(\mathbf{G}) = \frac{1}{\Omega_a} \int e^{-i\mathbf{G}\cdot\mathbf{r}} V_i^a(\mathbf{r}) d^3r, \quad (4)$$

where $V_i^a(\mathbf{r})$ is the local atomic pseudopotential and Ω_a is the atomic volume. The EPM bandstructure calculation requires the evaluation of the Hamiltonian matrix for a suitable set of basis functions, usually plane waves, followed by direct diagonalization.

The equations written above, common to the standard EPM approach, are applicable to a general periodic system, strained or unstrained. Now, in the standard derivation of the EPM, the assumption is made that the atomic pseudopotentials are spherical with the consequence that form factors $V_i(\mathbf{G})$ depend only upon the magnitude of the reciprocal lattice vectors, i.e., $V_i(\mathbf{G}) = V_i(G)$ where $G = |\mathbf{G}|$. Invoking this approximation leads to a considerable simplification of the problem. Since the pseudopotential need only be known at the reciprocal lattice vector magnitudes, G , and the magnitudes of the Fourier components are found to reduce sharply with G , the number of form factors that are required to provide a good description of unstrained bulk materials can be kept very small. Indeed only six form factors are generally used in most bulk calculations, and these can be easily fitted to available experimental data.²⁸ However, for strained systems, the spherical approximation restricts the degree to which the symmetry breaking effect of the strain

may be described, and eventually leads to conceptual difficulties in the meaning of the form factors.

An effective description of the reduced symmetry of strained systems may be achieved by removing the restriction to spherical symmetry. However, simply replacing the $V_i(G)$ by the $V_i(\mathbf{G})$ presents a significant problem in fixing the values of the form factors. Clearly, the number of distinct form factors has increased considerably, to a number impractical for fitting to empirical data. Further, these values must, in principle, be specified for each strain configuration required. A direct implementation of this approach is therefore inappropriate. What is required is a function $V_i(\mathbf{G})$, which incorporates the differences in the Fourier components along different directions, but which may easily be generated from the empirical information.

A practical solution to this problem, and that invoked in the EPM calculations in the present work, is to attempt to separate the form factor variations into components along the crystal axes. In this approach, the form factor function is defined by,

$$V(\mathbf{G}) = \frac{g_x^2}{|\mathbf{G}|^2} V_{a_x}(G^x) + \frac{g_y^2}{|\mathbf{G}|^2} V_{a_y}(G^y) + \frac{g_z^2}{|\mathbf{G}|^2} V_{a_z}(G^z), \quad (5)$$

where $\mathbf{G} = (g_x, g_y, g_z)$ and a_x , a_y and a_z are the lattice constants along the cubic crystal axes. The functions V_{a_i} are empirical potentials independently fitted for the bulk semiconductor hydrostatically strained to the lattice constant in the i th direction, a_i . These functions are evaluated at G^i , the magnitude of the reciprocal lattice vector corresponding to \mathbf{G} under hydrostatic strain to lattice constant a_i . For the calculation of the band structure for a strained bulk material, evaluation of the necessary Hamiltonian matrix elements requires only that bulk form factors are fitted to appropriate empirical data pertaining to hydrostatically strained bulk materials (i.e., strained to the lattice constants corresponding to the strained lattice constants along each of the crystal axes). At this point, it should be noted that the separation of the form factors in this way cannot be justified *a priori*, and the discrepancy introduced by this represents an approximation inherent to the method.

Direct implementation of Eq. (5) by refitting the potentials for each strain condition encountered is cumbersome for studies in which the same material may be studied in a variety of situations, e.g., grown on different substrates. It is convenient, therefore, to construct a generalized potential through interpolation between the form factors of a series of hydrostatic strains (lattice constants). For each hydrostatic strain condition, a set of six form factors are obtained (using typical cutoffs), corresponding to particular bulk reciprocal lattice vectors. Interpolating between the form factor associated with equivalent reciprocal lattice vectors at these strains enables the functions V_{a_i} to be generated for any intermediate strain required. In practice, it is found that a simple quadratic fit describes well the variation of the form factors with strain (see Fig. 1).

How can the method described above be extended to the study of superlattice structures? Equation (2) can be applied directly to the case of heterostructure systems, provided one takes care to note that the reciprocal lattice vectors \mathbf{G} are

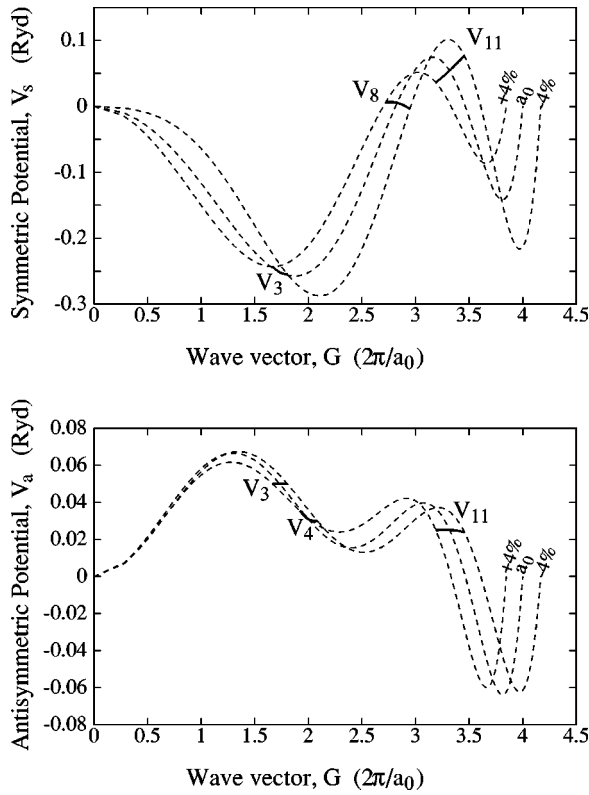


FIG. 1. The solid lines show the fit to the variation of the individual form factors with hydrostatic strain for InAs. The variation is shown in the symmetric and antisymmetric form factors over the range for which the change in lattice constant is -4% to $+4\%$ from the unstrained value. Also shown are the quintic polynomial fits used to describe the symmetric and antisymmetric pseudopotential at wave vectors intermediate to the bulk reciprocal lattice vectors, as required in calculating, for example, the superlattice pseudopotential.

then those of the unit cell of the heterostructure not the bulk. As a result, the reciprocal lattice vector lengths G at which the form-factor functions, V_{a_i} , must be evaluated, become less widely separated and take on a large number of values between those required for the case of bulk. In order that these functions may be evaluated at any intermediate values it is common practice to introduce an interpolation. The particular choice of interpolating function varies throughout the literature. In this paper, the method of Gell *et al.*,²⁷ using a quintic polynomial fit, is used. Note that this interpolation to intermediate values of reciprocal lattice vector length is performed between the individual strained form factors, which are themselves obtained by interpolation between the empirically fitted form factors of the hydrostatically strained bulk—this is illustrated in Fig. 1. The dimension of the Hamiltonian matrix, for a basis set of planes waves with given energy cutoff, increases linearly with the number of atoms in the unit cell, and soon limits the size of cell that can be practically studied. However, it is possible to exploit a knowledge of the nature of the system being studied to eliminate many of the basis functions that are not expected to contribute to the superlattice states of interest. In the calculations presented in this paper, only those basis functions with wavevectors lying within a given distance of bulk reciprocal lattice vectors are included in the basis set. This

process effectively restricts the superlattice states to contributions from bulklike states of near-zone-center character. Such a restriction is well established in EPM superlattice calculations adopting a linear combination of bulk bands approach.^{26,27} This approach enables the calculation of the superlattice states to be dramatically sped up, without loss of significant physics.

Finally, it is possible to extend the method further to address the problem of extremely large unit cells, containing several million atoms, in order to study the case of imperfect superlattice structures. To achieve this, a perturbation theory approach is adopted, whereby the wave functions of the imperfect superlattice, defined upon a large supercell, are expanded as a linear combination of strained (perfect) superlattice states. That is,

$$\Psi_{\mathbf{k}}^i = \sum_{n\mathbf{k}'} A_{n,\mathbf{k}'}^i \phi_{\mathbf{k}'}^n, \quad (6)$$

where $\Psi_{\mathbf{k}}^i$ is the wave function of the i th state of the imperfect superlattice, $\phi_{\mathbf{k}'}^n$ are the wave functions of the perfect superlattice at wave vectors $\mathbf{k}' = \mathbf{k} + \mathbf{g}$, and \mathbf{g} are the reciprocal lattice vectors of the supercell describing the imperfect superlattice. Defining U to be the perturbation potential for the imperfect superlattice, the Hamiltonian to be solved is $H = H_0 + U$. This leads to the secular equation,

$$A_{n',\mathbf{k}'}^i (E_{n',\mathbf{k}'}^0 - E^i) + \sum_{n\mathbf{k}} A_{n\mathbf{k}}^i \langle \phi_{n',\mathbf{k}'} | U | \phi_{n\mathbf{k}} \rangle = 0, \quad (7)$$

where $E_{n',\mathbf{k}'}^0$ is the unperturbed eigenvalue state $n'\mathbf{k}'$, E^i is the energy of the i th perturbed level. Again, the size of the problem may be significantly reduced by consideration of the physical nature of the problem, allowing only certain bands and wave vectors to be retained in the wave-function expansion. Since the disorder represents only a relatively small deviation from the perfect superlattice states, only a relatively small number of such states are required to describe well the perturbed state, and a large reduction in the problem size is achieved.

It is instructive to briefly contrast the method presented here with other approaches to the description of strained systems by empirical pseudopotentials that have been presented in the literature. In a recent paper,³¹ an attempt was made to describe strained superlattices without redefining the reciprocal lattice, accounting for the effects of strain through changes in the atomic positions and an adjustment to the form factors. One of the most common approaches is to attempt to derive a single interpolated curve to represent both the change in form factors due to strain, and the intermediate form factor values required for heterostructure calculations,^{12,29,30,32} retaining the spherical potential form. Although careful choice of the fitting functions can ensure that such methods are successful in particular materials, the widespread application of the technique is difficult. This difficulty arises because one is essentially attempting to describe with a single function two effects that have a distinct physical origin. The method presented in this paper critically makes the distinction between these two processes, and accounts for each one independently. An alternative method, in which the wave function of the supercell is described by a

basis set consisting of strained bulk bands, has recently been presented by Wang and Zunger.³³

III. SCATTERING THEORY

The strain-dependent empirical pseudopotential method introduced in the preceding section provides us with an accurate description of the stationary states in perfect and imperfect superlattice structures. However, as indicated previously, there is currently a demand for a theory that can describe the dynamical properties of realistic (i.e., imperfect) structures. The primary objective of this study is to develop a theoretical scheme whereby the stationary states of the imperfect superlattice may be linked to its dynamical properties, namely scattering cross sections and lifetimes. To this end, we invoke the quantum theory of scattering which enables us to extract the relevant dynamical information from the stationary state solutions to the full (perturbed) Hamiltonian of the imperfect superlattices.

In conventional studies of dynamic properties of heterostructures scattering theory is used to obtain transition rates to provide a description of the perturbed, imperfect system for which the stationary states cannot practically be obtained by diagonalization of the full Hamiltonian.³⁴ This approach has restricted the study of dynamics in complex systems such as semiconductor heterostructures either to the Born approximation (i.e., first-order perturbation theory), or to simplified models of the system in which the microscopic detail has been neglected. To the author's knowledge, no practical scheme exists in which the full microscopic features of the system can be included in a scattering model to n th order. In the theoretical approach that we outline below, a standard result of scattering theory, namely the transition matrix (T matrix), is applied in an unorthodox manner to exploit our ability to diagonalize the full Hamiltonian. The microscopic nature of the empirical pseudopotential method ensures that the full atomistic picture of structural imperfection is implicitly accounted for in our dynamical calculations.

Consider the case of an electron in a particular superlattice state, $\psi_{\mathbf{k}}^n$, with wave vector \mathbf{k} and miniband index n . In a standard result of scattering theory, the transition rate from $\psi_{\mathbf{k}}^n$ to another state $\phi_{\mathbf{k}'}^{n'}$, due to interaction with perturbation U may be written

$$Q(\mathbf{k}, \mathbf{k}') = \frac{2\pi}{\hbar} |\langle \phi_{\mathbf{k}'}^{n'} | T | \psi_{\mathbf{k}}^n \rangle|^2 \delta(E_{\mathbf{k}} - E_{\mathbf{k}'}), \quad (8)$$

where the transition-matrix elements $\langle \phi_{\mathbf{k}'}^{n'} | T | \psi_{\mathbf{k}}^n \rangle$ are defined by

$$\langle \phi_{\mathbf{k}'}^{n'} | T | \psi_{\mathbf{k}}^n \rangle = \langle \phi_{\mathbf{k}'}^{n'} | U | \Psi_{\mathbf{k}}^n \rangle, \quad (9)$$

and the state $\Psi_{\mathbf{k}}^n$ is the (perturbed) evolution state of $\psi_{\mathbf{k}}^n$. The energy delta function in Eq. (8) restricts the transition rate to that of elastic scattering processes, where the scatterer has no internal degrees of freedom. The lifetime of the initial state may be obtained by considering transitions to all available states, and is given by

$$\tau_{n\mathbf{k}}^{-1} = \frac{2\pi}{\hbar} \sum_{n'\mathbf{K}} |\langle \phi_{\mathbf{K}}^{n'} | U | \Psi_{\mathbf{k}}^n \rangle|^2 \rho_{n'\mathbf{K}}(E_{n'\mathbf{K}}), \quad (10)$$

where $\Omega_{\mathbf{k}}$ is the volume of the Brillouin zone. In writing this expression it has been assumed that the transition-matrix elements remain virtually constant over small volumes of reciprocal space so that the integral over destination states may be separated into a summation of such volumes, thus:

$$\rho_{n'\mathbf{K}}(E_{n'\mathbf{K}}) = \Omega_{\mathbf{k}}^{-1} \int_{\Omega_{\mathbf{k}}} d\mathbf{k}' \delta(E_{n\mathbf{k}} - E_{n'\mathbf{k}'}) \quad (11)$$

where $\rho_{n'\mathbf{K}}(E_{n'\mathbf{K}})$ is the partial density of states in volume $\Omega_{\mathbf{K}}$ around wave vector \mathbf{K} .

In practical implementation of this scheme, using the wave functions obtained from the empirical pseudopotential method, it is necessary to deal carefully with the periodicity implicit in the pseudopotential model employed. The periodic nature of the supercell potential as modeled presents difficulties in the evaluation of Eq. (10). Nonzero matrix elements can only arise between wave vectors \mathbf{K} and \mathbf{k}' where they are separated by a reciprocal lattice vector of the system — as a result the probability of exact elastic scattering between states becomes negligible, and the lifetime tends to infinity. However, since the period of the supercell is much larger than the extent of the scattering potential, one can move conceptually to a continuum picture by taking the discrete \mathbf{k} points to represent a sampling of a continuous reciprocal space. Practically, this involves evaluation of the matrix elements by interpolation between the transition strengths at the discrete grid of points of the periodic system. Physically, this is equivalent to approximating to a unit cell of infinite extent. For such a system, involving scattering from a single localized potential, the lifetime no longer represents a well defined quantity; rather, one wishes to compute the scattering cross section associated with that impurity potential. The scattering cross section $\sigma_n(\mathbf{k})$ is defined,

$$\sigma_n(\mathbf{k}) = \frac{\Omega}{v_0^{n\mathbf{k}}} \frac{1}{\tau_{n\mathbf{k}}}, \quad (12)$$

where v_0 is the initial electron velocity and Ω is the normalization box volume. A convergent expression for $\sigma_n(\mathbf{k})$ is obtained upon substitution of Eq. (10) for the lifetime:

$$\sigma_n(\mathbf{k}) = \frac{2\pi}{\hbar} \frac{\Omega}{v_0^{n\mathbf{k}}} \sum_{n'\mathbf{K}} \left| \sum_{n,\mathbf{k}''} A_{n,\mathbf{k}''}^i \langle \phi_{\mathbf{K}}^{n'} | U | \phi_{\mathbf{k}''}^n \rangle \right|^2 \rho_{n'\mathbf{K}}(E_{n'\mathbf{K}}). \quad (13)$$

Here, the perturbed wave function has been written in the form of Eq. (6) — this form lends itself to the computation of the cross section, since the wave vectors \mathbf{k}'' are precisely those wave vectors that are involved in the supercell perturbation calculation, so the matrix elements of U required to calculate $\sigma_n(\mathbf{k})$ have already been evaluated in obtaining the solution to the perturbed Hamiltonian.

Having thus obtained an expression for the cross section of a single scattering center, we can proceed to the case of a random arrangement of such scatterers, sufficiently far apart as to be effectively isolated. In this instance it is the overall cross section, proportional to the total number of centers,

which diverges. On the other hand, the lifetime of such a system is well defined, and applying Eq. (12) once more, for a total of N_{SC} scattering centers, the microscopic expression for the lifetime may be written,

$$(\tau_{n\mathbf{k}})^{-1} = \frac{2\pi}{\hbar} N_{SC} \sum_{n'\mathbf{K}} \left| \sum_{n,\mathbf{k}''} A_{n,\mathbf{k}''}^i \langle \phi_{\mathbf{K}}^{n'} | U | \phi_{\mathbf{k}''}^n \rangle \right|^2 \rho_{n'\mathbf{K}}(E_{n'K}). \quad (14)$$

This expression converges for a given density of scattering centers, since the dependence on crystal volume of the number of scattering centers and partial density of states is exactly cancelled by the normalization of the wave functions.

Finally, we note that Eqs. (13) and (14), derived from the T matrix using the perturbed wave functions, include all n th-order scattering processes. First-order expressions, equivalent to the results of Fermi's Golden Rule, may be obtained by repeating the above derivation with the perturbed evolution state, $\Psi_{\mathbf{k}}^n$, approximated by the leading term in its expansion, simply $\psi_{\mathbf{k}}^n$. This leads to first-order expressions for the cross section and lifetime,

$$\sigma_n(\mathbf{k}) = \frac{2\pi}{\hbar} \frac{\Omega}{v_0} \sum_{n'\mathbf{K}} |\langle \phi_{\mathbf{K}}^{n'} | U | \phi_{\mathbf{k}}^n \rangle|^2 \rho_{n'\mathbf{K}}(E_{n'K}), \quad (15)$$

$$(\tau_{n\mathbf{k}})^{-1} = \frac{2\pi}{\hbar} N_{SC} \sum_{n'\mathbf{K}} |\langle \phi_{\mathbf{K}}^{n'} | U | \phi_{\mathbf{k}}^n \rangle|^2 \rho_{n'\mathbf{K}}(E_{n'K}), \quad (16)$$

which include only single scattering processes.

IV. RESULTS

A. Perfect $\text{Ga}_{0.75}\text{In}_{0.25}\text{Sb}/\text{InAs}$ superlattice

The superlattice structure chosen for the present study is the $11\text{Ga}_{0.75}\text{In}_{0.25}\text{Sb}/9\text{InAs}$ structure (where 9InAs represents 9 monolayers, 4.5 lattice constants, of InAs) pseudomorphically grown on GaSb , studied experimentally by Jack *et al.*³⁵ This structure is typical of recently proposed detector structures, and the methods applied here would also be applicable across a wide range of heterostructure configurations. Indeed, the present work forms part of an on-going project in which the dynamical properties of a large number of antimonide-based heterostructures are to be characterized.

Before proceeding to the results of calculations relating to structural imperfections, it is instructive to examine the fundamental properties of the ideal heterostructure specified above. The band-edge alignment for this structure, calculated using the model solid approach of Van de Walle,³⁶ is illustrated schematically in Fig. 2. This shows that the structure is a type-II broken-gap (sometimes referred to as type III) superlattice, in which the top of the alloy valence band lies above the InAs conduction minimum. For such an alignment the superlattice will have a nonzero energy gap only for sufficiently narrow layers, in which case the energies due to quantum confinement in the valence and conduction wells are sufficient to lower the alloy valence-band edge below the InAs conduction-band edge. This is the case for the $11\text{Ga}_{0.75}\text{In}_{0.25}\text{Sb}/9\text{InAs}$ structure studied.

The electronic band structure of the $11\text{Ga}_{0.75}\text{In}_{0.25}\text{Sb}/9\text{InAs}$ superlattice was calculated using the strain-dependent empirical pseudopotential method de-

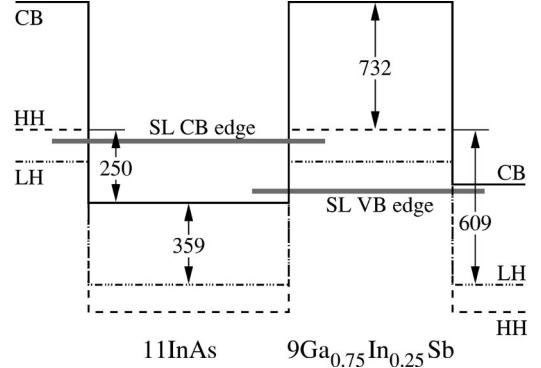


FIG. 2. The broken-gap band alignment in the $\text{InAs}/\text{Ga}_{0.75}\text{In}_{0.25}\text{Sb}$ superlattice grown on GaSb , including the effects of strain, with numerical values (meV) calculated using the method of Van de Walle (Ref. 36). The conduction (CB), heavy-hole (HH), and light-hole (LH) band line-ups are shown. The positions of the conduction- and valence-band edges for the type-II $11\text{InAs}/9\text{Ga}_{0.75}\text{In}_{0.25}\text{Sb}$ structure are indicated.

scribed in Sec. II. The strain-dependent pseudopotentials were fitted to the experimental data,³⁷ and the alloy was described using the virtual crystal approximation (VCA),³⁸ in which the alloy layer is described by a potential with full zinc-blende symmetry and properties interpolated between those of the constituent materials. In a very recent paper,³⁹ the empirical pseudopotential method described in this paper was used to study the effect of the VCA on the optical response of heterostructures. For the purposes of the present study, the VCA shall be assumed, though inclusion of alloy disorder effects will form a natural extension to the work in the present paper. Figure 3 shows the computed charge densities associated with the states at the zone center, plotted down the center of the spiral in the superlattice growth direction. The general confinement of the valence and conduction minibands to different layers is clearly seen, though it is

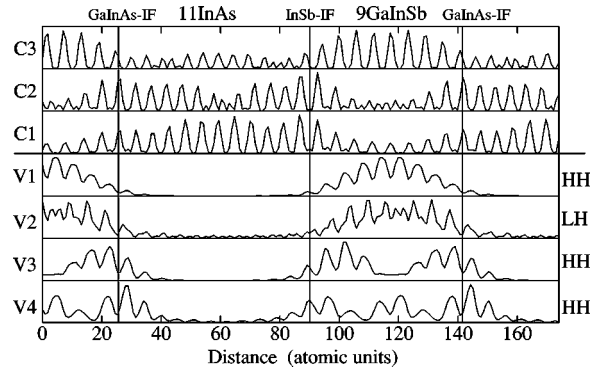


FIG. 3. The charge densities (arbitrary units) associated with the zone-center states close to the fundamental gap of the $11\text{InAs}/9\text{Ga}_{0.75}\text{In}_{0.25}\text{Sb}$ superlattice are plotted against distance in the growth direction, averaged over spin-degenerate pairs. The charge densities are plotted along the center of the atomic spirals lying along the direction of superlattice growth, for the highest four valence minibands, and lowest three conduction minibands. The valence minibands have been identified as ground heavy-hole (HH1), ground light-hole (LH1), and first- and second-excited heavy-hole minibands (HH2, and HH3, respectively). The two different interface bonding types are indicated.

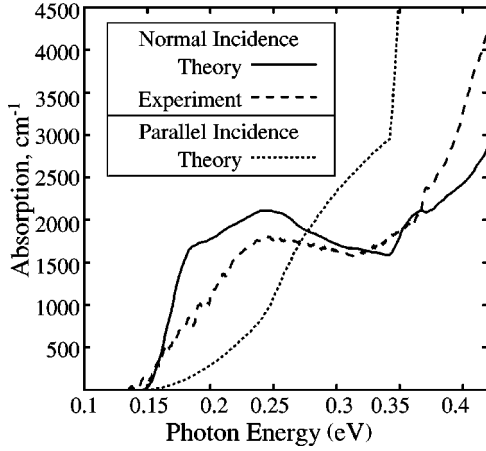


FIG. 4. The variation of the calculated normal incidence absorption coefficient (cm^{-1} , solid lines) with photon energy (eV) for the $11\text{InAs}/9\text{Ga}_{0.75}\text{In}_{0.25}\text{Sb}$ superlattice is compared with the experimental result of Jack *et al.* (Ref. 35) (dashed lines) for a nominally identical structure. Also shown for comparison is the calculated parallel incidence (zz polarization) absorption.

also apparent that there is a relatively large degree of wave-function leakage in the conduction band. This leakage results in an enhanced wave-function overlap, necessary to obtain a reasonably strong interband transition close to the fundamental gap, in turn needed for improved infrared detection. The microscopic nature of the EPM description is indicated by the clear distinction in Fig. 3 between the two different interface types, present in the superlattice, $\text{Ga}_{0.75}\text{In}_{0.25}\text{As}$ -like and InSb -like.

The optical absorption spectra for this structure were computed by sampling the superlattice band structure to evaluate the microscopic expression for the absorption coefficient obtained from density matrix theory.⁴⁰

$$\begin{aligned} \chi_{\mu\alpha}^{(1)}(-\omega_\sigma; \omega_1) = & -\frac{e^2 N}{Vm\epsilon_0\omega_\sigma\omega_1} \delta_{\mu\alpha} \\ & + \frac{e^2}{Vm^2\epsilon_0\hbar\omega_\sigma\omega_1} \sum_k \sum_a f_0(a) \\ & \times \sum_b \left[\frac{P_{ab}^\mu P_{ba}^\alpha}{(\Omega_{ba} - i\gamma - \omega_1)} \right. \\ & \left. + \frac{P_{ab}^\alpha P_{ba}^\mu}{(\Omega_{ba} + i\gamma + \omega_1)} \right]. \end{aligned} \quad (17)$$

A tetrahedral interpolation procedure was used to obtain a convergent expression, and the sampling was restricted to the active region of the Brillouin zone as detailed in the literature.⁴¹ Figure 4 shows the computed spectrum for normal incidence (xx polarization) absorption and parallel incidence (zz polarization) absorption. Also shown is the experimental normal incidence absorption (xx polarization) spectrum measured by Jack *et al.*³⁵ The excellent agreement between the theoretical and experimental absorption spectrum provide evidence that the EPM calculations provide a good description of both the electronic energies (determining the cutoff energies) and the transition probabilities (dictating the magnitude of the response).

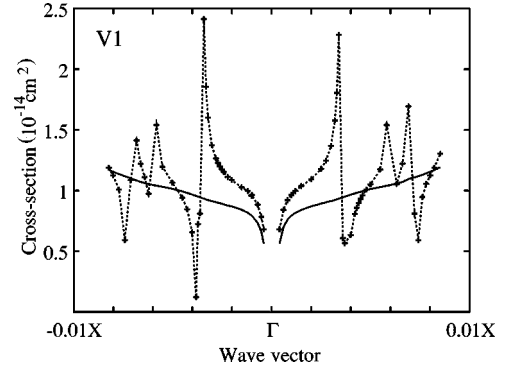


FIG. 5. The wave-vector dependence of the hole scattering cross section (10^{-14}cm^2) of a 49Sb_{As} defect island, radius two lattice constants, height of two anion layers and 50% swapping fraction. The cross section is shown for the uppermost hole miniband. The dashed lines show the result of the full calculation including multiple scattering events (the crosses indicate the wave vectors at which the cross section was calculated), while the solid lines show the first-order, Born approximation, contribution.

Having thus examined the behavior of the idealized superlattice, it remains to apply the theoretical framework developed in Sec. III to investigate the properties of imperfect superlattice structures.

B. Interface islands of isovalent anion defects

Let us consider now the case of a superlattice as defined in the previous section, but with substitutional isovalent anion defects in the form of interface islands. In particular, the case of cylindrical islands adjacent to the $\text{Ga}_{0.75}\text{In}_{0.25}\text{As}$ -like interfaces is considered, with a fraction x of all anions inside the island swapped from As to Sb (denoted Sb_{As} defects).

Initially, the variation of scattering cross section with incident carrier wave vector was studied in detail for an island sufficiently deep to contain two layers of As atoms, and with a radius of two lattice constants. A fraction of 50% of the As anions are replaced randomly by Sb anions resulting in an island containing 49Sb_{As} defects. The calculated wave-vector dependence of the cross section is shown in Fig. 5, for initial states in the highest valence miniband, and in Fig. 6, for the lowest conduction miniband. The cross section was calculated using both the n th order T -matrix theory [Eq. (13)], and in the first-order (golden rule) approximation [Eq. (15)], and the results of these two approaches may be compared in Figs. 5 and 6. It is clear that there is a considerable contribution to the wave-vector dependence of the cross-section due to higher-order (multiple scattering event) processes, though it is also apparent that the characteristic magnitude of the cross section is rather well described by the simpler golden rule calculations in which only single-scattering events are included. The higher-order contribution appears as a resonance structure superimposed upon the first-order scattering response.

The calculations were repeated for a large number of cylindrical island defect configurations of the type described above. As the intention here is to investigate the broad dependence of the cross section upon the specifications of the defect island, it is sufficient to compare the cross section calculated according to the golden rule, which while not able

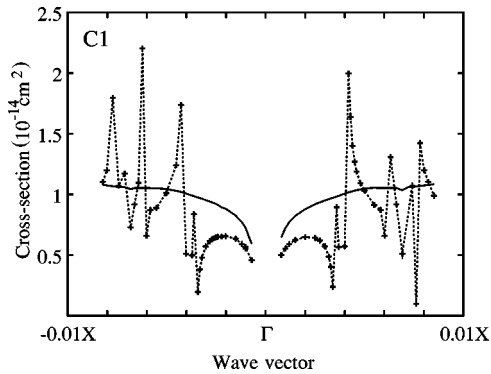


FIG. 6. The wave-vector dependence of the electron scattering cross section (10^{-14} cm^2) of a 49 Sb_{As} defect island, radius two lattice constants, height of two anion layers and 50% swapping fraction. The cross section is shown for the lowest conduction miniband. The dashed lines show the result of the full calculation including multiple scattering events (the crosses indicate the wave vectors at which the cross section was calculated), while the solid lines show the first-order, Born approximation, contribution.

to reproduce the fine wave-vector-dependent variation, does reflect the overall scattering strength of the defect. The variation of this cross section, at a particular wave vector of $\approx 0.005X$, is shown in Fig. 7 as the radius of islands is changed. The cross section is plotted on a logarithmic scale against the number of defect anions in the island. Points representing islands with a given height have been connected by solid lines to indicate the variation of the cross section with radius. The straight lines obtained indicate that the cross section obeys a simple power-law variation with the number of defect atoms. Analysis of the gradients of the lines gives values of 1.83 for height of one atom, and 1.98 for height of three. The form of Eq. (15) suggests that, in the zeroth order approximation, one might expect that the cross section will assume an n^2 dependence. From the above discussion, the results of the full calculation indicate that as the radius is increased the actual variation is rather close to this naive expectation. However, in contrast, the solid lines in Fig. 8 connect points representing islands of given radius, illustrating the dependence on island height. It is clear that in this

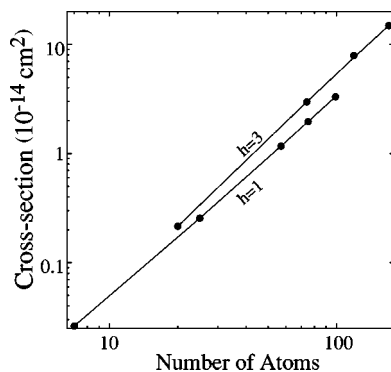


FIG. 7. The scattering cross section (10^{-14} cm^2) of cylindrical islands of varying height and radius (all with 50% anions swapped), plotted against the number of Sb_{As} defects in the island. Lines are drawn through points representing islands of heights sufficient to contain 1 anion layer, $h=1$, and 2 anion layers, $h=2$, as the island radius is varied.

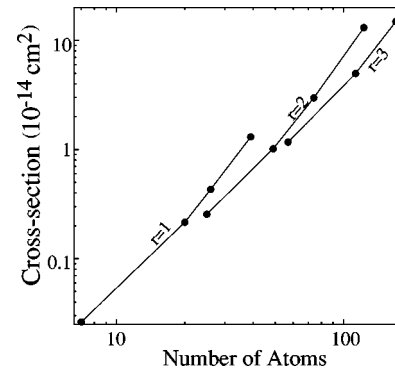


FIG. 8. The scattering cross section (10^{-14} cm^2) of cylindrical islands of varying height and radius (all with 50% anions swapped), plotted against the number of Sb_{As} defects in the island. Lines are drawn through points representing islands of radii, r (lattice constants) as the island height is varied.

case the variation goes beyond a simple power law. It can be concluded that the effectiveness of the islands as scatterers is enhanced in the case of islands that protrude the greatest distance into the layer.

Of course, the true variations in the cross section must include the effect of higher-order contributions, themselves dependent on the detailed composition of the defects. As is clear from the dispersion relations in Figs. 5 and 6, the nature of the higher-order contribution is highly sensitive to the wave vector. It is interesting to consider how the relative contribution of the higher-order terms in the T matrix formalism, reflecting the multiple scattering events, depends upon the size and shape of the defects. As might be expected, the relative influence of the higher-orders increases as the strength of the first-order scattering itself increases. At a wave vector of $0.003X$, for example, the multiple scattering terms alter the cross-section by 40% for islands with first-order cross section of $\approx 1 \times 10^{-14} \text{ cm}^2$, while for a single anion defect, with first-order strength $\approx 1 \times 10^{-18} \text{ cm}^2$ the relative change is less than 0.1%. This suggests that the use of Fermi's golden rule introduces considerable inaccuracies as the islands become larger—the precise magnitude of the relative error due to this approximation is sensitive to the wave vector at which the cross section is evaluated.

C. Single-anion defects

It is now interesting to consider the case of isolated substitutional anion defects, i.e., to take the limiting case of islands containing just a single defect. Figure 9 shows the wave-vector dependence of the cross section for a single- Sb_{As} defect adjacent to the interface, for initial states in the highest two valence and lowest two conduction minibands. For these defects the golden rule and T matrix give indistinguishable results. Comparison with the dispersion relations for the 49 atom island in Figs. 5 and 6 indicates that the form of the wave-vector dependence for the single defect is similar to the first-order contribution to the larger island, though the scattering strength is three orders of magnitude smaller.

In a very recent paper⁴² the scattering from isolated substitutional anion defects adjacent to the interfaces was shown to be highly sensitive to the nature of the defect: i.e., the

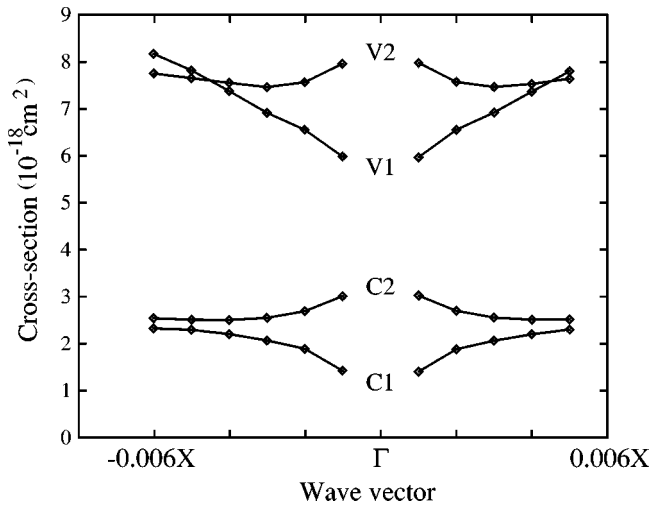


FIG. 9. The wave-vector dependence of the electron scattering cross section (10^{-18} cm^2) of an isolated Sb_{As} defect at the $\text{Ga}_{0.75}\text{In}_{0.25}\text{As}$ -like interface. The cross section is shown for the lowest conduction miniband (C1) and next lowest (C2), and for the uppermost (V1) and next highest (V2) valence minibands.

magnitude of the cross section depended upon whether Sb_{As} or As_{Sb} defects were present. What is the microscopic origin of the difference between these defects, and to what extent does the scattering depend upon the proximity to the heterostructure interfaces? To address these questions a systematic study of the changes in scattering properties with the position of these defects, and of the effect of the relaxation of the lattice around the defects, is presented.

First, consider the scattering of electrons occupying states in the lowest conduction miniband, and for clarity consider only those electrons with a particular wave vector of $\approx 0.005X$. The cross section was computed for single anion defects at each of the anion sites available in the unit cell of an ideal $11\text{Ga}_{0.75}\text{In}_{0.25}\text{Sb}/9\text{InAs}$ superlattice. The results are shown in Fig. 10, where the results of calculations involving full lattice relaxation are compared to those obtained with

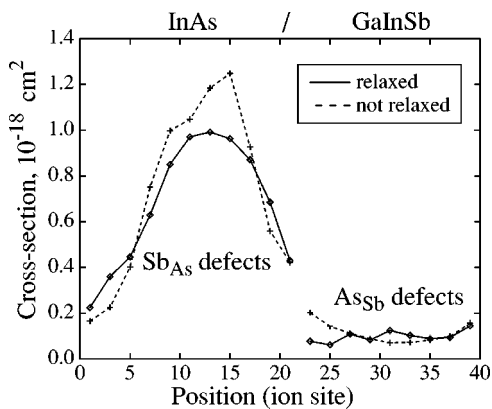


FIG. 10. The cross section (10^{-18} cm^2) for electrons in the lowest conduction miniband is plotted against the position of single isovalent substitutional anion defects. For positions labeled 1 to 21 these correspond to Sb_{As} defects, while for labels greater than 21 they represent As_{Sb} defects. The solid lines show the cross section calculated with full relaxation of the lattice around the defect, while the dashed lines show the variation when the lattice is frozen.

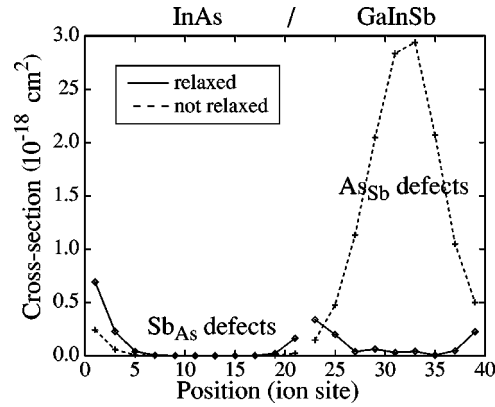


FIG. 11. The cross section (10^{-18} cm^2) for holes in the uppermost valence miniband is plotted against the position of single isovalent substitutional anion defects. For positions labeled 1 to 21 these correspond to Sb_{As} defects, while for labels greater than 21 they represent As_{Sb} defects. The solid lines show the cross-section calculated with full relaxation of the lattice around the defect, while the dashed lines show the variation when the lattice is frozen.

fixed atom positions. In Fig. 10, the anion sites in the InAs layers (corresponding to Sb_{As} defects) are shown on the left-hand side of the diagram, while the sites in the $\text{Ga}_{0.75}\text{In}_{0.25}\text{Sb}$ layers (corresponding to As_{Sb} defects) are shown on the right-hand side. The scale on the position axis refers to labels of the atoms in the unit cell, starting at 1 for the As anion forming part of the GaInAs-like interface, to 40 for the GaIn cation at the other end of the unit cell. The Sb_{As} defects occupy odd-numbered sites up to 21, while the As_{Sb} defects occupy odd sites from 23. The form of these results is consistent with the expectations of a simple envelope function picture: the peak in electron scattering occurs at the center of the InAs layer, reflecting the greater overlap of the electronic wave function with the defect perturbation. The As_{Sb} defects scatter the electrons only weakly since the electrons are confined to the other layers of the superlattice. Further, note that the relaxation of the atoms around the defect has only a very small effect on the peak of the electron cross section.

However, in the case of the scattering from the highest hole miniband, a rather surprising result is obtained. Figure

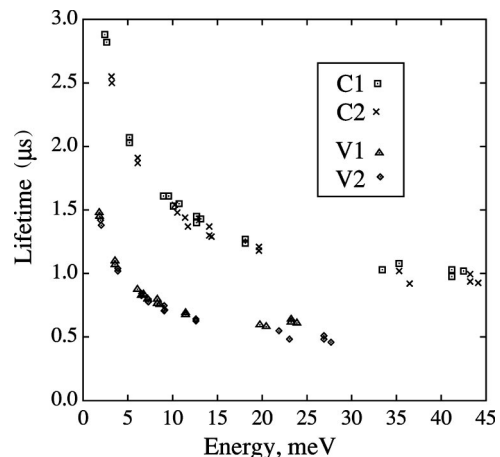


FIG. 12. The lifetime (μs), calculated for 10^{16} cm^{-3} isolated Sb_{As} impurities, plotted as a function of the carrier energy relative to the band edge (meV) for electrons in the lowest two conduction minibands, C1 and C2, and highest two valence minibands, V1 and V2.

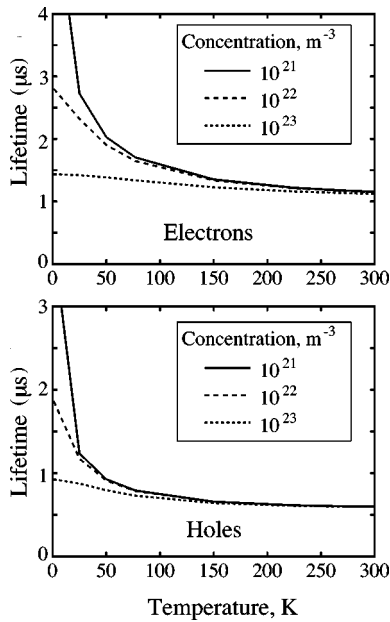


FIG. 13. The average lifetime (μs) calculated for an ensemble of electrons and holes in a structure with 10^{16} cm^{-3} isolated Sb_{As} impurities, plotted as a function of temperature (K). The lifetimes are shown for carrier concentrations of 10^{21} m^{-3} , 10^{22} m^{-3} , and 10^{23} m^{-3} .

11 shows the cross section for scattering from initial hole states, and again compares for relaxed and unrelaxed atom positions. For the calculations with no relaxation of the atoms, the variation of the cross section is once again consistent with the envelope-function description of the wave functions. This time the maximum scattering occurs at the center of the valence well since that is where the hole wave function has greatest overlap with the defect potential. However, upon relaxation of the atoms there is a quite radical change to the cross section of the As_{Sb} defects. The relaxation results in the whole central peak of cross section being eliminated, leaving maxima directly adjacent to the interfaces (where in fact relaxation enhances the scattering). Further analysis, by computing the effective cross section due to the defect atom itself due to the surrounding atoms separately, indicates that the relaxation of the alloy atoms around the defect gives rise to a large out-of-phase contribution to the cross section, which nearly cancels the scattering from the defect itself. Clearly this deviation from the envelope-function picture can only be described by a full microscopic model of the defect and the scattering process, such as that presented here.

Why is the effect of the relaxation so different between the two types of defect? The peak in electron cross section remains strong under relaxation of the surrounding InAs, but the peak of the hole cross section is virtually eliminated by the relaxation of the alloy atoms. One possible explanation would be that the nature of the relaxation is different — examination of the change in atom positions shows that while the magnitude of the atomic movement is similar in each case, the direction of movement is different. Around the Sb_{As} defect the InSb bonds formed are very much longer than the InAs bonds and the lattice breathes out, while the As_{Sb} defect in the alloy results in shorter GaAs and InAs bonds giving rise to an inward movement of atoms. In fact,

by modeling the physically unrealistic structures obtained by forcing the atoms around the Sb_{As} defect to relax inwards (as though around the As_{Sb}), and *vice versa* it was found that the direction of relaxation was *not* the origin of the discrepancy. Rather, it was found that the difference in the effect of relaxation around the particular defect atoms arose principally from the difference in the host materials in which they exist — in other words, it is simply a property of the $\text{Ga}_{0.75}\text{In}_{0.25}\text{Sb}$ alloy that it gives a large contribution to the cross section when its atoms are moved.

D. Carrier lifetimes

For semiconductor heterostructures a more relevant indicator than the cross section is the scattering lifetime, which may be calculated from Eq. (14). In order to evaluate the lifetime it is necessary to specify some concentration of the scattering centers concerned. In the present calculations a concentration of scattering centers of 10^{16} cm^{-3} is assumed. For isolated Sb_{As} defects adjacent to the $\text{Ga}_{0.75}\text{In}_{0.25}\text{As}$ interface, at this concentration the carrier scattering lifetime is shown as a function of incident energy (relative to the band edges) in Fig. 12. The lifetimes corresponding to initial electron and hole states are shown. It can be seen that there is a strong energy dependence to the variation of lifetime. Consequently, in order to compute a characteristic lifetime for a given ensemble of carriers, it is necessary to consider its distribution throughout the bands: that is, to account for the different occupations of states of particular energies. Such consideration results in a lifetime dependent upon both the concentration of carriers for which the lifetime is to be determined, and their temperature.

By considering a particular concentration of electron- or hole-carriers in the band, and imparting a Fermi-Dirac distribution for a given temperature, the effective ensemble lifetimes were calculated for a number of defects. Figure 13 shows the variation of the lifetime against temperature for several different carrier populations. At higher temperatures the average lifetimes decrease as the carriers are excited to higher energies, moving away from the Brillouin zone center, and occupy states with shorter lifetimes (see Fig. 12). As might be expected, the sensitivity of the lifetime to such redistribution of carriers is greater for small overall carrier concentrations. At higher temperatures the effective lifetime is essentially determined by the lifetimes of higher energy states, and the lifetime becomes insensitive to changes in population.

For the single- Sb_{As} defects at the $\text{Ga}_{0.75}\text{In}_{0.25}\text{As}$ interfaces, the lifetime at 77 K of a population of 10^{16} cm^{-3} electrons is $1.6 \mu\text{s}$. However, for the same defects located at the center of the well, the lifetime reduces to just $0.35 \mu\text{s}$. It is clear, then, that the scattering lifetime is determined not only by the size and chemical species of the defects but also by the precise location of the defects relative to the interfaces. A more dramatic change in lifetime may be seen if one considers the effect of defects forming into clusters. For the 49Sb_{As} island considered previously, the lifetime drops to just 0.4 ns —the factor of 49 increase in density of defects is reflected by a 4000 times reduction in the lifetime. This reduction in the lifetime is still not sufficient to make the elastic scattering from these defects comparable to the lifetimes

from processes such as interface roughness scattering, ionized impurity scattering, and phonon scattering. However, it should be noted that the concentrations of defects considered are not as large as those observed experimentally.^{22,23} For larger islands or higher island densities the lifetime might be reduced to compete with other processes. In these cases the effect of islanding observed may be significant in determining the device characteristics. The calculations presented here provide a benchmark for the strength of these elastic scattering processes at the given defect concentrations.

It is interesting to compare the lifetimes associated with the As_{Sb} defects, at the interfaces and at the center of the alloy layer. In this case, the lifetime drops from $4.9 \mu s$ at the interface to $3.1 \mu s$ at the center of the well. Thus it can be seen that the shortest lifetimes due to Sb_{As} defects are an order of magnitude less than that of the As_{Sb} defect. The origin of this difference was analyzed in comparison of the scattering cross sections in the previous section. The implication of this result for optimization of device structures is clear, namely that the elimination of excess antimony should be a priority for improvement of lifetimes in these structures.

V. CONCLUSION

The theoretical scheme developed in this paper addresses first the requirement for a microscopic description of the states in imperfect strained antimonide-based superlattices, and second the need for a microscopic account of the dynamical properties governing the performance of devices made from these heterostructures. An empirical pseudopotential scheme with strain-dependent potentials satisfies the demand for microscopic wave functions while scattering theory provides the link to the device indicators such as carrier lifetimes.

In this paper, the theory has been applied to the particular case of a $Ga_{0.75}In_{0.25}Sb/InAs$ superlattice in the presence of a range of isovalent anion defects. It has been shown that the

scattering cross section and carrier lifetime are sensitive to the detailed nature of the imperfections: the chemical species of the defect(s), the location of the defects relative to the interfaces, the formation of defects into interface islands. Further, the role of lattice relaxation has been identified, and leads to a variation of cross section with defect location qualitatively different to the expectations of a simple envelope-function model. The contribution of multiple scattering processes is shown to exhibit a strong wave-vector dependence, and to become significant for larger interface islands. Only a full microscopic theory is able to describe even the qualitative details of the factors governing the lifetime. For typical concentrations of defects and electrons, and at a temperature of 77 K, the lifetime of isolated substitutional antimony defects is calculated to be $1.6 \mu s$ for defects adjacent to the interfaces, and $0.35 \mu s$ at the center of the InAs layer. The minimum lifetime associated with arsenic defects in the alloy layers is $3.1 \mu s$, implying that the elimination of excess antimony is more important with regard to device performance. For antimony interface islands of approximately 50 atoms the lifetime reduces to the subnanosecond regime.

In establishing a link between the microscopic defect configuration the dynamical macroscopic properties relevant to practical applications, the theory developed in this study can provide vital information on the factors limiting device performance. While the theory has been demonstrated for a particular superlattice in this paper, it is a generic tool applicable to a wide range of heterostructures and defect types.

ACKNOWLEDGMENTS

I would like to thank the Office of Naval Research (U.S.A.), the U.K. Engineering and Physical Science Research Council, and D. E. R. A. (Malvern) for financial support. I also thank M. Jaros for many helpful discussions.

-
- ¹H. Mohseni, J. Wojkowski, M. Razeghi, and W. Mitchel, *IEEE J. Quantum Electron.* **35**, 1041 (1999).
- ²L. J. Olafsen, E. H. Aifer, I. Vurgaftman, W. W. Bewley, C. L. Felix, J. R. Meyer, D. Zhang, C. -H. Lin, and S. S. Pei, *Appl. Phys. Lett.* **72**, 2370 (1998).
- ³J. R. Meyer, L. J. Olafsen, E. H. Aifer, W. W. Bewley, C. L. Felix, I. Vurgaftman, M. J. Yang, L. Goldberg, D. Zhang, C. -H. Lin, S. S. Pei, and D. H. Chow, *IEE Proc.: Optoelectron.* **145**, 275 (1998).
- ⁴I. Vurgaftman, J. R. Meyer, and L. R. Ram-Mohan, *IEEE J. Quantum Electron.* **34**, 147 (1998).
- ⁵R. M. Biefield, A. A. Allerman, and S. R. Kurtz, *Mater. Sci. Eng., B* **51**, 1 (1998).
- ⁶H. Q. Lei, C. H. Lin, and S. S. Pei, *Appl. Phys. Lett.* **72**, 3434 (1998).
- ⁷M. J. Yang, W. J. Moore, B. R. Bennett, and B. V. Shanabrook, *Electron. Lett.* **34**, 270 (1998).
- ⁸W. W. Bewley, E. H. Aifer, C. L. Felix, I. Vurgaftman, J. R. Meyer, C. -H. Lin, S. J. Murray, D. Zhang, and S. S. Pei, *Appl. Phys. Lett.* **71**, 3607 (1997).
- ⁹J. I. Malin, J. R. Meyer, C. L. Felix, J. R. Lindle, L. Goldberg, C. A. Hoffman, F. J. Bartoli, C. -H. Lin, P. C. Chang, S. J. Murray, R. Q. Yang, and S. S. Pei, *Appl. Phys. Lett.* **68**, 2976 (1996).
- ¹⁰R. H. Miles, D. H. Chow, Y.-H. Zhang, P. D. Brewer, and R. G. Wilson, *Appl. Phys. Lett.* **66**, 1921 (1995).
- ¹¹A. N. Baranov, N. Bertru, Y. Cuminal, G. Boissier, C. Alibert, and A. Joullié, *Appl. Phys. Lett.* **71**, 735 (1997).
- ¹²C. Jenner, E. A. Corbin, B. M. Adderley, and M. Jaros, *Semicond. Sci. Technol.* **13**, 359 (1998).
- ¹³M. H. Young, D. H. Chow, A. T. Hunter, and R. H. Miles, *Appl. Surf. Sci.* **128**, 395 (1998).
- ¹⁴H. Mohseni, E. Michel, J. Sandoen, M. Razeghi, W. Mitchel, and G. Brown, *Appl. Phys. Lett.* **71**, 1403 (1997).
- ¹⁵J. L. Johnson, L. A. Samoska, A. C. Gossard, J. L. Mertz, M. D. Jack, G. R. Chapman, B. A. Baumgratz, K. Kosai, and S. M. Johnson, *J. Appl. Phys.* **80**, 1116 (1996).
- ¹⁶F. Szmulowicz, E. R. Heller, K. Fisher, and F. L. Madarasz, *Superlattices Microstruct.* **17**, 373 (1995).
- ¹⁷I. H. Campbell, I. Sela, B. K. Laurich, D. L. Smith, C. R. Bolognesi, L. A. Samoska, A. C. Gossard, and H. Kroemer, *Appl. Phys. Lett.* **59**, 846 (1991).

- ¹⁸D. H. Chow, R. H. Miles, J. R. Söderström, and T. C. McGill, *Appl. Phys. Lett.* **56**, 1418 (1990).
- ¹⁹B. R. Bennett, M. J. Yang, B. V. Shanabrook, J. B. Boos, and D. Park, *Appl. Phys. Lett.* **72**, 1193 (1998).
- ²⁰E. R. Brown, E. R. Söderström, J. R. Parker, L. J. Mahoney, K. M. Molvar, and T. C. McGill, *Appl. Phys. Lett.* **58**, 2291 (1991).
- ²¹B. Z. Noshov, W. H. Weinberg, J. J. Zinck, B. V. Shanabrook, B. R. Bennett, and L. J. Whitman, *J. Vac. Sci. Technol. B* **16**, 2381 (1998).
- ²²J. Harper, M. Weimer, D. Zhang, C.-H. Lin, and S. S. Pei, *Appl. Phys. Lett.* **73**, 2805 (1998).
- ²³J. Harper, M. Weimer, D. Zhang, C. -H. Lin, and S. S. Pei, *J. Vac. Sci. Technol. B* **16**, 1389 (1998).
- ²⁴M. J. Shaw, *Phys. Rev. B* **58**, 7834 (1998).
- ²⁵L.-W. Wang, S.-H. Wei, T. Mattila, A. Zunger, I. Vurgaftman, and J. R. Meyer, *Phys. Rev. B* **60**, 5590 (1999).
- ²⁶M. Jaros, K. B. Wong, and M. A. Gell, *Phys. Rev. B* **31**, 1205 (1985).
- ²⁷M. A. Gell, K. B. Wong, D. Ninno, and M. Jaros, *J. Phys. C* **19**, 3821 (1986).
- ²⁸M. L. Cohen and T. K. Bergstresser, *Phys. Rev.* **141**, 789 (1966).
- ²⁹I. Morrison, M. Jaros, and K. B. Wong, *Phys. Rev. B* **35**, 9693 (1987).
- ³⁰P. Friedel, M. S. Hybertsen, and M. Schlüter, *Phys. Rev. B* **39**, 7974 (1988).
- ³¹G. C. Dente and M. L. Tilton, *J. Appl. Phys.* **86**, 1420 (1999).
- ³²K. A. Mäder and A. Zunger, *Phys. Rev. B* **50**, 17 393 (1994).
- ³³L.-W. Wang and A. Zunger, *Phys. Rev. B* **59**, 15 806 (1999).
- ³⁴J. Callaway, *Energy Band Theory* (Academic Press, New York, 1964).
- ³⁵M. D. Jack, B. A. Baumgratz, G. R. Chapman, S. M. Johnson, J. L. Johnson, L. A. Samoska, A. C. Gossard, and J. L. Mertz (private communication).
- ³⁶C. G. Van de Walle, *Phys. Rev. B* **39**, 1871 (1989).
- ³⁷*Zahlenwerte und Funktionen aus Naturwissenschaften und Technik*, edited by K. H. Hellwege, Landolt-Börnstein, New Series, Group III, Vols. 17a and 22a (Springer, New York, 1982).
- ³⁸M. Jaros, *Rep. Prog. Phys.* **48**, 1091 (1985).
- ³⁹M. R. Kitchin, M. J. Shaw, E. A. Corbin, J. P. Hagon, and M. Jaros, *Appl. Surf. Sci.* (to be published).
- ⁴⁰P. N. Butcher and T. P. McLean, *Proc. Phys. Soc. London* **81**, 219 (1963).
- ⁴¹M. J. Shaw, G. Gopir, P. R. Briddon, and M. Jaros, *J. Vac. Sci. Technol. B* **16**, 1794 (1998).
- ⁴²M. J. Shaw, J. P. Hagon, E. A. Corbin, and M. Jaros, *J. Vac. Sci. Technol. B* **17**, 2025 (1999).